Journal of Controlled Release xxx (2016) xxx–xxx

Contents lists available at ScienceDirect

Journal of Controlled Release

journal homepage: www.elsevier.com/locate/jconrel

$\alpha_v\beta_3$ Integrin-targeted reduction-sensitive micellar mertansine prodrug: Superb drug loading, enhanced stability, and effective inhibition of melanoma growth in vivo

Ping Zhong, Hao Meng, Jie Qiu, Jian Zhang, Huanli Sun, Ru Cheng *, Zhiyuan Zhong *

Biomedical Polymers Laboratory, and Jiangsu Key Laboratory of Advanced Functional Polymer Design and Application, College of Chemistry, Chemical Engineering and Materials Science, Soochow University, Suzhou 215123, PR China

ARTICLE INFO

Article history:
Received 8 December 2016
Accepted 11 December 2016
Available online xxxx

Keywords:
Mertansine
Prodrug
cRGD
Reduction-responsive
Targeted chemotherapy

ABSTRACT

Antibody-maytansinoid conjugates (AMCs) have emerged as one of the most promising active targeting cancer therapeutics. Their clinical use is, however, challenged by their low drug content, poor stability, high cost and potential immune response. Here, we designed and developed robust, cRGD-functionalized, reduction-sensitive polymeric micellar mertansine (DM1) prodrug (cRGD-MMP) that showed targeted treatment of B16F10 melanoma-bearing C57BL/6 mice. cRGD-MMP was obtained with a superb drug content of ~40 *wt.%* and a small size of ~45 nm from poly(ethylene glycol)-*b*-(poly(trimethylene carbonate)-*graft*-SSDM1) (PEG-P(TMC-*g*-SSDM1)) and cRGD-functionalized PEG-P(TMC-*g*-SSDM1) copolymers. cRGD-MMP exhibited excellent stability in 10% fetal bovine serum and cell culture medium while fast swelling and markedly accelerated drug release under a reductive environment. Confocal microscopy, flow cytometry and MTT assays indicated receptor-mediated uptake and high antitumor effect of cRGD-MMP in $\alpha_v\beta_3$ integrin over-expressing B16F10 melanoma cells. Notably, cRGD-MMP displayed a long elimination half-life of 5.25 h and 4-fold better maximum-tolerated dose than free DM1. The *in vivo* studies demonstrated that cRGD-MMP effectively inhibited B16F10 melanoma growth and greatly improved mice survival rate as compared to free DM1 and non-targeted MMP control. cRGD-MMP with superior stability, drug loading, and $\alpha_v\beta_3$ targetability offers an attractive alternative to AMCs for malignant tumor therapy.

1. Introduction

Mertansine (DM1) is a powerful tubulin polymerization inhibitor that can effectively treat various malignancies including breast cancer, melanoma, multiple myeloma and lung cancer [1,2]. The recent FDA approval of Kadcyla® (ado-trastuzumab emtansine) for the treatment of HER2-positive metastatic breast cancer inspired intensive development of antibody-maytansinoid conjugates (AMCs) for different malignancies [3–5]. Notably, there are nearly ten types of AMCs have entered various phases of clinical trials [6–8]. AMCs have emerged as one of the most promising active targeting cancer therapeutics. It has to be noted, however, that the clinical use of AMCs, as for other antibody-drug conjugates (ADCs), is challenged by their low drug content, poor stability, high cost, small scale production, and potential immunogenicity [9–11].

Water soluble polymer-drug conjugates, analogous to ADCs, can effectively improve drug solubility, blood circulation time, and drug toleration [12–17]. Unlike ADCs, polymer-drug conjugates usually possess a low immunogenicity and can be easily produced in a large scale. A couple of polymer-drug conjugates such as polyglutamic acid conjugated paclitaxel (PGA-PTX) and poly(N-(2-hydroxylpropyl) methacrylamide)-doxorubicin conjugates (HPMA-DOX) have been translated to the clinical trials [18–21]. The overall therapeutic effects of polymer-drug conjugates are low, partly resulting from their too small size (<10 nm), poor tumor accumulation and inefficient tumor cell uptake [22,23]. In recent years, polymeric micellar prodrugs, which combine the virtues of both polymer-drug conjugates and nano-micelles, have attracted increasing interests for cancer therapy [24–30]. For instance, Torchilin et al. developed a MMP2-sensitive paclitaxel-conjugated micellar nanoparticles with low risk of drug leakage that exhibited enhanced anticancer activity in vitro and in a A549 xenografted mouse model [29]. We reported a hyaluronic acid-shelled pH-activatable micellar PTX prodrug that showed potent inhibition of CD44-overexpressing MCF-7 human breast tumor xenografts [30].

Here, we designed and developed a robust, cRGD-functionalized, reduction-sensitive polymeric micellar mertansine prodrug (cRGD-MMP) for targeted treatment of B16F10 melanoma-bearing C57BL/6 mice (Scheme 1). cRGD-MMP is *co*-self-assembled from poly(ethylene glycol)-*b*-(poly(trimethylene carbonate)-*graft*-SSDM1) (PEG-P(TMC-*g*-SSDM1)) and cRGD-functionalized PEG-P(TMC-*g*-SSDM1) copolymers.

* Corresponding authors.
E-mail addresses: rcheng@suda.edu.cn (R. Cheng), zyzhong@suda.edu.cn (Z. Zhong).

http://dx.doi.org/10.1016/j.jconrel.2016.12.011
0168-3659/

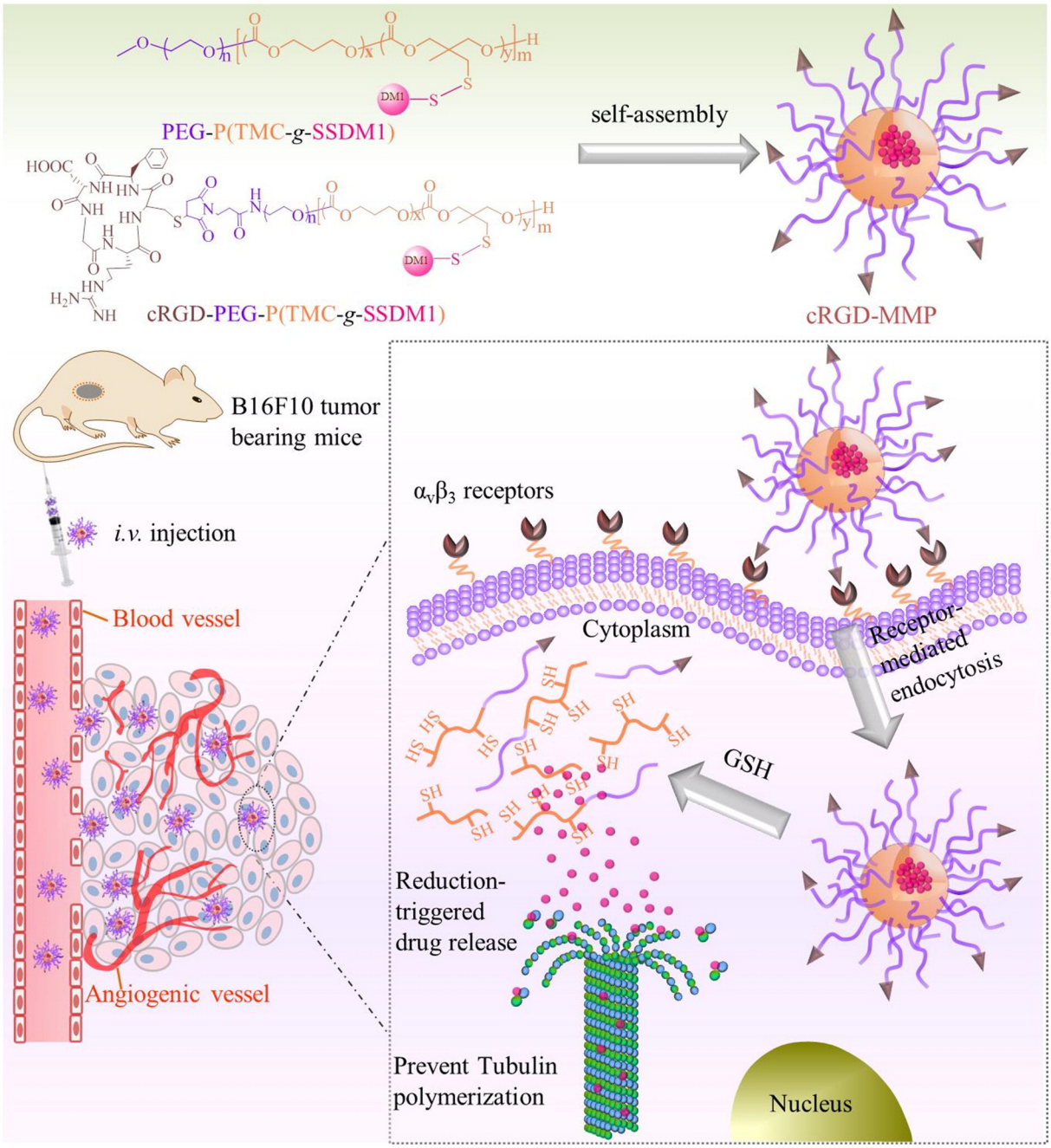

Scheme 1. Schematic illustration of cRGD-functionalized, reduction-sensitive micellar mertansine prodrug (cRGD-MMP) for targeted treatment of B16F10 melanoma-bearing C57BL/6 mice. cRGD-MMP was co-self-assembled from PEG-P(TMC-*g*-SSDM1) and cRGD-functionalized PEG-P(TMC-*g*-SSDM1) copolymers.

DM1, a thiol-containing maytansinoid [31], is grafted to polycarbonate backbone via a disulfide bond that can be cleaved under a reductive condition, leading to fast cytoplasmic release of pristine DM1. Various reduction-sensitive nanosystems have recently been explored for triggered intracellular drug release [32–38]. PTMC is a well-established synthetic biomedical materials that possess excellent biocompatibility, biodegradability and flexibility [39,40]. The cyclic arginine-glycine-aspartate (cRGD) peptide has shown a strong binding affinity toward $\alpha_v\beta_3$ integrin overexpressed on angiogenic endothelial cells and several malignant cancer cells such as glioblastoma and melanoma [41–46]. It should be noted that several antibody-maytansinoid conjugates with a disulfide linker have advanced to phase I–II clinical trials [10,47]. The disulfide linkage in these AMCs, however, turned out too labile in blood circulation. In the present work, disulfide bonds and DM1 are designed to locate in the micellar core, which is expected to afford a high stability and reduced premature drug release. To the best of our knowledge, this is a first report on smart micellar mertansine prodrug that possesses a superb drug loading, high stability, active tumor targetability and internalization, and accelerated intracellular drug release.

2. Materials and methods

2.1. Materials

Methoxy poly(ethylene glycol) (PEG-OH M_n = 5.0 kg/mol, Fluke) was dried by azeotropic distillation from anhydrous toluene before use. Trimethylene carbonate (TMC, Jinan Daigang Biomaterial Co., Ltd.) was purified through recrystallizing from dry ethyl acetate before use. Zinc bis[bis(trimethylsilyl) amide] (97%, Aldrich), cyclo(RGD*f*C) (cRGD-SH, 98%, China Peptides Co., Ltd.), maleimide poly(ethylene

glycol) (Mal-PEG-OH, M_n = 5.0 kg/mol, Creative PEGWorks), glutathione (GSH, 99%, Roche), N_2'-deacetyl-N_2'-(3-mercapto-1-oxopropyl)-maytansine (DM1, >98%, Suzhou BrightGene Co., Ltd.), and glacial acetic acid (GR, Sinopharm Chemical Reagent Co., Ltd.) were used as received. Dichloromethane (DCM) and *N*, *N*-dimethylformamide (DMF) were purified by the solvent purification system (Innovative Technology) before use. Pyridyldisulfide cyclic carbonate monomer (PDSC) was prepared according to a previously reported procedure [48].

2.2. Synthesis of PEG-P(TMC-co-PDSC) copolymer

PEG-P(TMC-*co*-PDSC) copolymer was synthesized by ring-opening polymerization of TMC and PDSC with PEG-OH as an initiator and zinc bis[bis(trimethylsilyl) amide] as a catalyst. Typically, in a glove-box under a nitrogen atmosphere, to a Schlenk bottle equipped with a magnetic stir bar were charged PEG-OH (100 mg, 20 μmol), TMC (81.6 mg, 800 μmol), PDSC (86.7 mg, 320 μmol) and DCM (1.9 mL). Then, a DCM stock solution of zinc bis[bis(trimethylsilyl) amide] (3.85 mg, 10 μmol) was added. The reaction proceeded at 40 °C for 24 h. PEG-P(TMC-*co*-PDSC) copolymer was obtained by precipitation in excess cold diethyl ether, filtration and drying in vacuum. Yield: 81.5%. ^{1}H NMR (400 MHz, $CDCl_3$): PEG: δ 3.37, 3.64; TMC: δ 4.24, 2.04; PDSC: δ 8.46, 7.65, 7.09, 4.10, 3.01, 1.12. M_n (^{1}H NMR) = 11.8 kg/mol, M_n (GPC) = 23.3 kg/mol, M_w/M_n = 1.53.

2.3. Synthesis of PEG-P(TMC-g-SSDM1) prodrug

PEG-P(TMC-*g*-SSDM1) prodrug was prepared via thiol-disulfide exchange reaction between PEG-P(TMC-*co*-PDSC) and DM1. Under a nitrogen atmosphere, to PEG-P(TMC-*co*-PDSC) (150 mg, 0.133 mmol of pyridyl disulfide group) and DM1 (145.3 mg, 0.197 mmol) in anhydrous DMF (28 mL) was added a catalytic amount of glacial acetic acid. The reaction proceeded at 35 °C for 48 h. The reaction was monitored by UV–vis measurement (374 nm, UH5300, HITACHI, JAPAN) of pyridine-2-thione. The resulting PEG-P(TMC-*g*-SSDM1) prodrug was purified via extensive dialysis (Spectra/Pore, MWCO 7000) against DMF and then deionized water and lyophilized. Yield: 75%. ^{1}H NMR (600 MHz, DMSO-d_6): PEG: δ 3.09, 3.50; TMC: δ 4.13, 1.94; DM1: δ 7.16, 6.89, 6.54, 5.92, 5.56, 5.30, 4.53, 3.12–3.55, 1.94 and 0.71–1.52. M_n (^{1}H NMR) = 17.5 kg/mol.

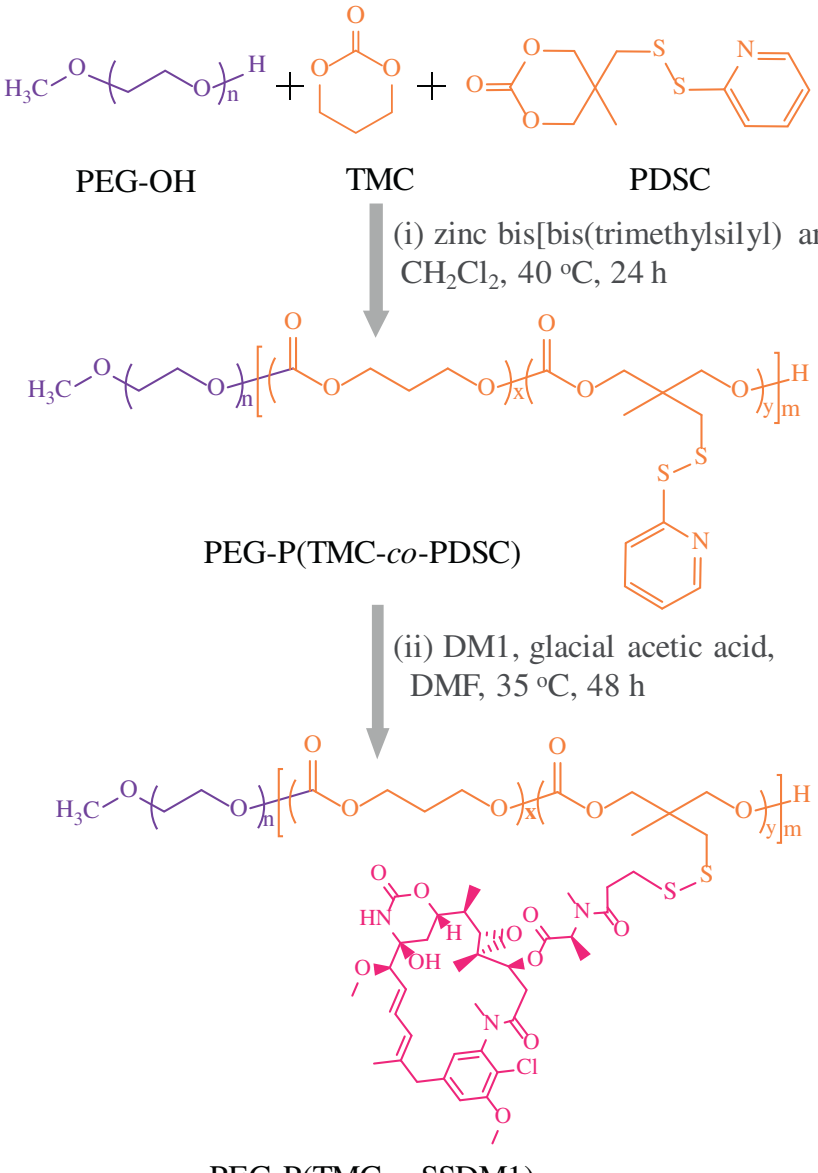

Scheme 2. Synthesis of PEG-P(TMC-*g*-SSDM1) copolymer.

Please cite this article as: P. Zhong, et al., αvβ3 Integrin-targeted reduction-sensitive micellar mertansine prodrug: Superb drug loading, enhanced stability, and effective i..., J. Control. Release (2016), http://dx.doi.org/10.1016/j.jconrel.2016.12.011

2.4. Synthesis of cRGD-PEG-P(TMC-g-SSDM1) prodrug

cRGD-PEG-P(TMC-*g*-SSDM1) prodrug was prepared in three steps. Firstly, Mal-PEG-P(TMC-*co*-PDSC) copolymer was synthesized in the same manner as for PEG-P(TMC-*co*-PDSC), except that Mal-PEG-OH (M_n = 5.0 kg/mol, Creative PEGWorks) was used as a macro-initiator. Yield: 82.3%. ^{1}H NMR (400 MHz, $CDCl_3$): PEG: δ 3.63; TMC moieties: δ 4.23, 2.05; PDSC moieties: δ 8.46, 7.65, 7.09, 4.10, 3.01, 1.12, Mal group: δ 6.71. M_n (^{1}H NMR) = 12.0 kg/mol, M_n (GPC) = 26.1 kg/mol, M_w/M_n = 1.42. Secondly, cRGD-PEG-P(TMC-*co*-PDSC) copolymer was obtained by conjugating cRGD-SH to Mal-PEG-P(TMC-*co*-PDSC) micelles that were prepared by solvent-exchange method. Mal-PEG-P(TMC-*co*-PDSC) solution (80 mg, 6.67 μmol) in DMF (4 mL) was added dropwise into PB buffer (16 mL, 10 mM, pH 7.4), followed by extensive dialysis (Spectra/Pore, MWCO 3500). After 10 min degassing, cRGD-SH (6.92 mg, 10 μmol) was added under a nitrogen atmosphere.

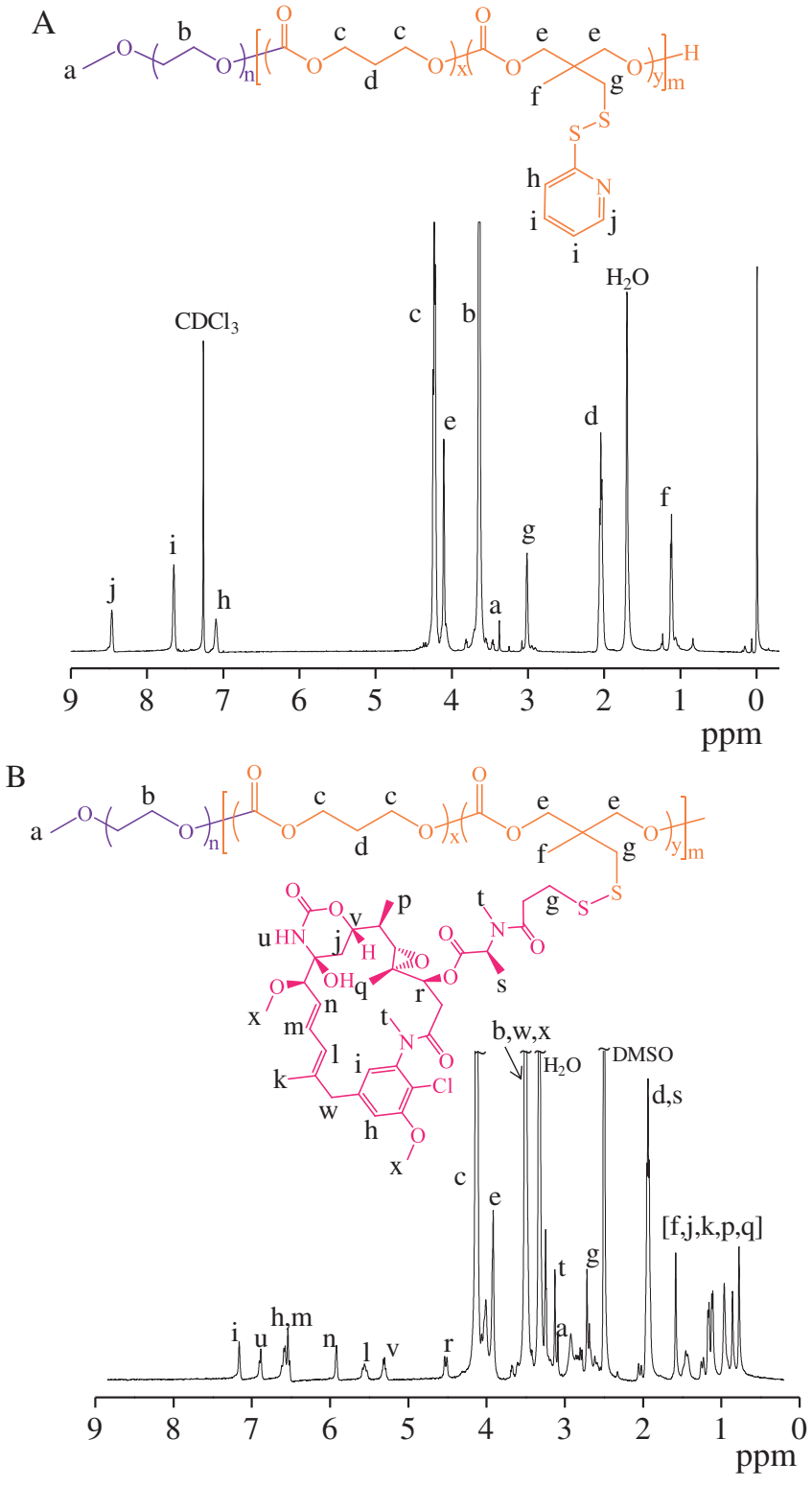

Fig. 1. ^{1}H NMR spectra of PEG-P(TMC-*co*-PDSC) (400 MHz, $CDCl_3$) (A) and PEG-P(TMC-*g*-SSDM1) (600 MHz, DMSO-d_6) (B).

Please cite this article as: P. Zhong, et al., αvβ3 Integrin-targeted reduction-sensitive micellar mertansine prodrug: Superb drug loading, enhanced stability, and effective i..., J. Control. Release (2016), http://dx.doi.org/10.1016/j.jconrel.2016.12.011

The reaction proceeded at room temperature for 24 h. cRGD-PEG-P(TMC-*co*-PDSC) was isolated by extensive dialysis (Spectra/Pore, MWCO 3500) against deionized water to remove free cRGD-SH and lyophilization. Yield: 78%. ^{1}H NMR (400 MHz, DMSO-d_6): PEG: δ 3.50; TMC: δ 4.12, 1.93; PDSC: δ 8.44, 7.80, 7.71, 7.21, 4.06, 3.01, 1.01. Finally, cRGD-PEG-P(TMC-*g*-SSDM1) prodrug was synthesized via thiol-disulfide exchange reaction with DM1 as for PEG-P(TMC-*g*-SSDM1) prodrug. Yield: 73%. ^{1}H NMR (600 MHz, DMSO-d_6): PEG: δ 3.50; TMC: δ 4.13, 1.94; DM1: δ 7.16, 6.89, 6.54, 5.92, 5.56, 5.30, 4.53, 3.12–3.55, 1.94 and 0.71–1.52. M_n (^{1}H NMR) = 17.9 kg/mol.

2.5. Colloidal stability and reduction-sensitivity of cRGD-MMP

The stability of cRGD-MMP in 10% fetal bovine serum (FBS) and Dulbecco's modified Eagle's medium (DMEM) was studied by DLS over 24 h. FBS solution was filtrated with 210 nm filter before use.

The reduction-sensitivity of cRGD-MMP was studied by DLS under shaking (200 rpm) at 37 °C through monitoring its size change in response to 10 mM GSH over time. cRGD-MMP dispersion without GSH was used as a control.

2.6. In vivo pharmacokinetic studies

The mice were all handled under protocols approved by Soochow University Laboratory Animal Center and the Animal Care and Use Committee of Soochow University. The pharmacokinetics of cRGD-MMP and MMP were studied in C57BL/6 mice (DM1 dosage: 5 mg DM1 equiv./kg). After administration, the blood samples were collected at 0.083, 0.5, 0.75, 1, 2, 4, 8, 12, or 24 h post injection of cRGD-MMP or MMP. Each blood sample was dissolved in 0.2 mL of methanol. cRGD-MMP or MMP was extracted by incubating blood samples in 0.5 mL of DMSO under shaking (200 rpm) at 37 °C for one day. Excess DTT (50 mM) was added to each vial to release DM1. The amount of DM1 in the supernatant was determined by HPLC. The results were presented as mean ± standard deviation (n = 4).

2.7. Evaluation of maximum-tolerated dose (MTD)

SPF female normal C57BL/6 mice with body weights in the range of 18–22 g were used to evaluate the MTD of cRGD-MMP and MMP. The mice were *i.v.* injected with cRGD-MMP or MMP at a single dose ranging from 4, 6 to 8 mg DM1 equiv./kg. The body weights, survival rates as well as other indicators such as abnormal behaviors, anomalous secretions or pupil, abnormal phenomena noted in skin and hair of mice were monitored over 10 days. MTD was defined as the maximum dosage of DM1 that leads to no >15% body weight loss and no other remarkable toxicities during the entire ten days [49]. The results were presented as mean ± standard deviation (n = 5).

2.8. In vivo antitumor efficacy

The in vivo antitumor efficacy of cRGD-MMP and MMP was studied using malignant B16F10 tumor model established by subcutaneously injecting 8×10^6 B16F10 cells in 50 μL of serum-free DMEM media to the hind flank of nude mice. When the tumor sizes reached around 30 mm^3 after 5 days implantation, the mice were weighted and randomly divided into six groups (n = 8) and this day was designated as day 0. The mice were intravenously administrated every two days for a total of three injections via tail vein with PBS (blank control), free DM1 at 0.8 mg/kg, MMP at 2.4 mg DM1 equiv./kg and cRGD-MMP at 0.8, 1.6 or 2.4 mg DM1 equiv./kg, respectively. Tumor sizes were recorded using calipers and calculated based on the following formula: V = 0.5 × L × W × H, where L, W and H are the longest, widest and highest directions in tumor dimension [50]. The relative tumor volumes were

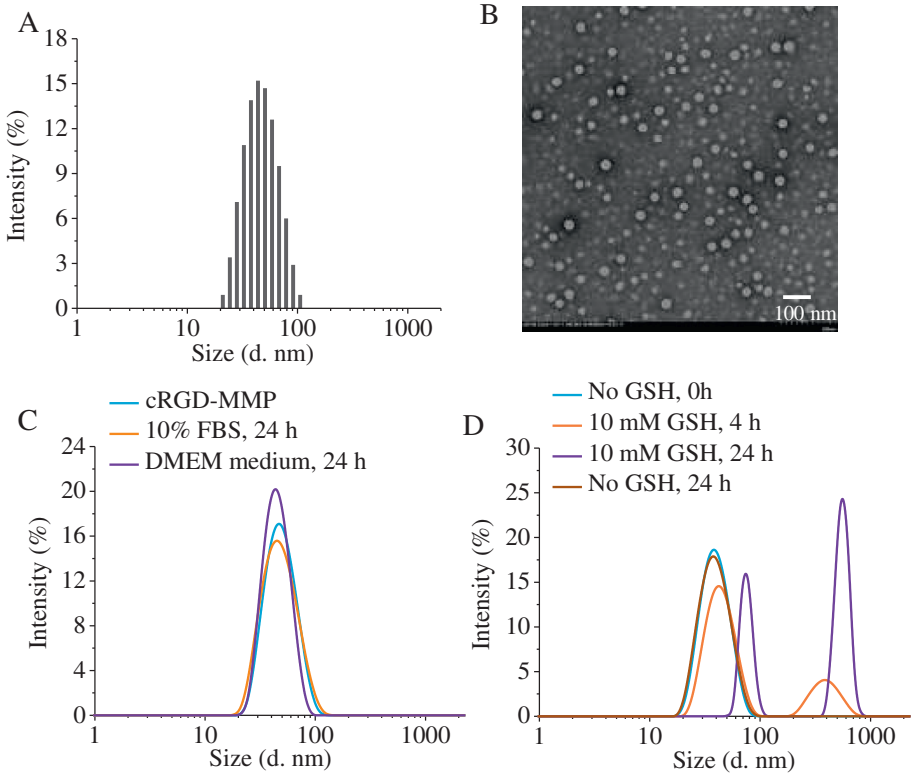

Fig. 2. Size distribution of cRGD-MMP determined by DLS (A) and TEM (B); (C) Colloidal stability of cRGD-MMP against 10% FBS and DMEM culture medium; (D) Size change of cRGD-MMP in response to 10 mM GSH.

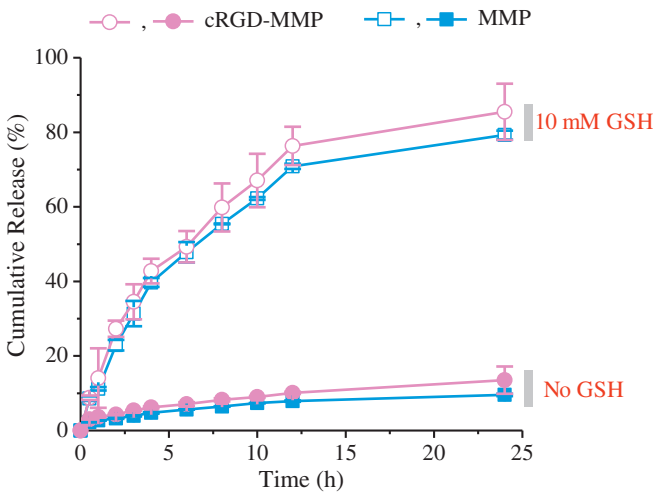

Fig. 3. Cumulative release behaviors of DM1 from cRGD-MMP and MMP in PB (pH 7.4, 10 mM) with or without 10 mM GSH (micelle concentration: 0.8 mg/mL).

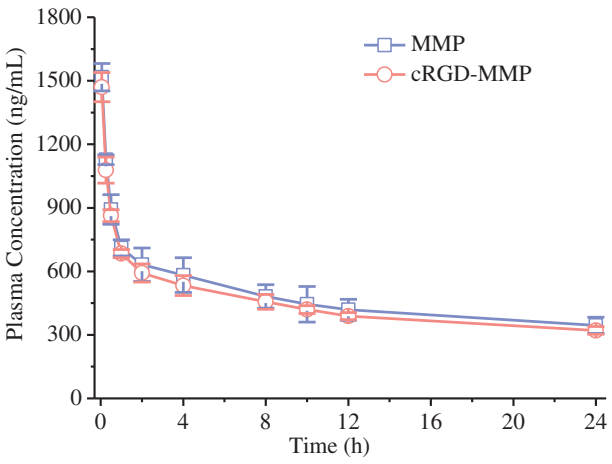

Fig. 5. In vivo pharmacokinetics of cRGD-MMP and MMP in C57BL/6 mice (dose: 5 mg DM1 equiv./kg). The results were presented as mean ± standard deviation (n = 4).

given as the tumor size at each time point divided by that at day 0. The mice were weighed every two days. At day 10, three mice of each group were sacrificed and tumors were harvested and weighed, the remained five mice of each group were used to monitor the survival time. Tumor inhibition rate (TIR) was calculated according to the following formulus: (1- (mean tumor weight of DM1 treated group/mean tumor weight of saline treated group)) × 100.

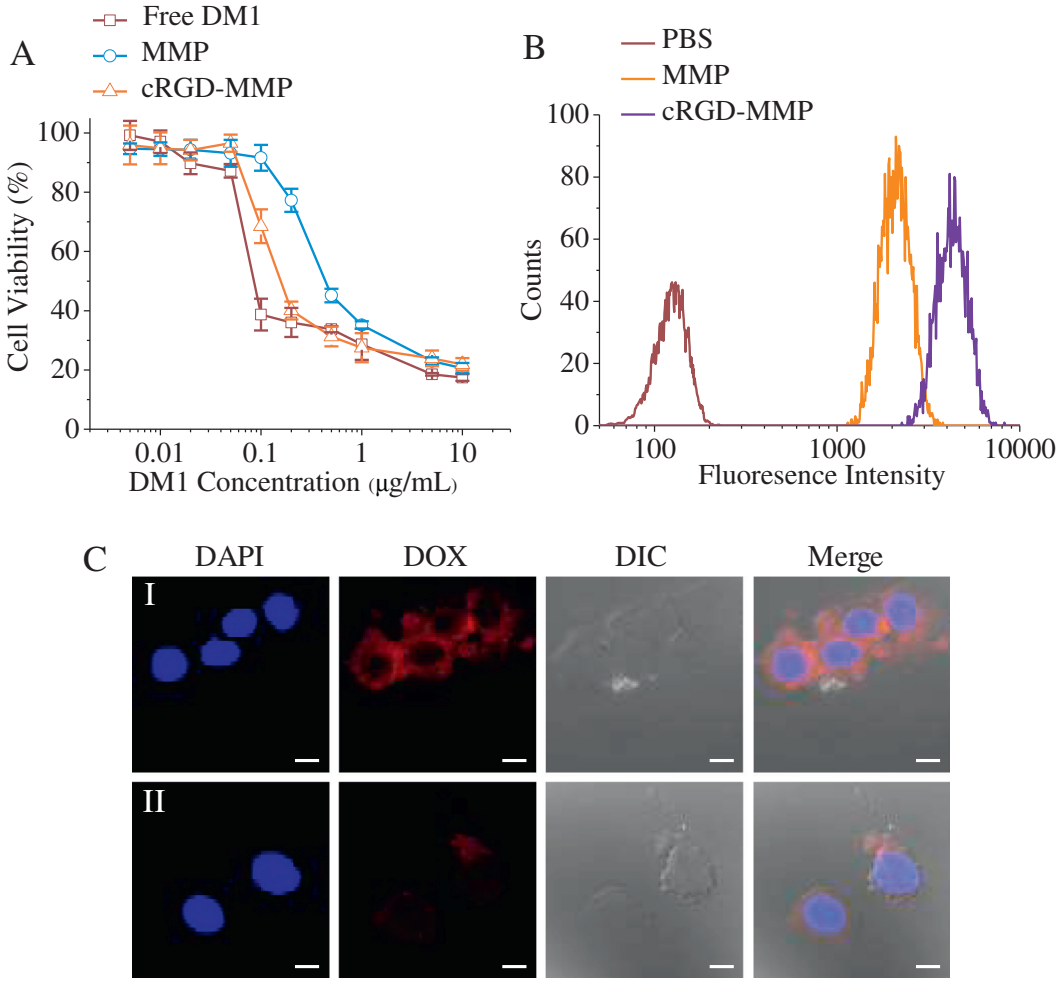

Fig. 4. (A) The in vitro cytotoxicity of free DM1, cRGD-MMP and MMP to B16F10 cells determined by MTT assays. The results were presented as mean ± standard deviation (n = 4); (B) Flow cytometry of B16F10 cells following 4 h incubation with DOX-loaded cRGD-MMP or DOX-loaded MMP. (C) CLSM images of B16F10 cells following 4 h incubation with DOX-loaded cRGD-MMP (I) or DOX-loaded MMP (II) (scale bar: 10 μm). For each panel, the images from left to right show cell nuclei stained by DAPI (blue), DOX fluorescence in B16F10 cells (red), the differential interference contrast microscopy (DIC) of cells and overlays of the three images. (For interpretation of the references to color in this figure legend, the reader is referred to the web version of this article.)

Please cite this article as: P. Zhong, et al., αvβ3 Integrin-targeted reduction-sensitive micellar mertansine prodrug: Superb drug loading, enhanced stability, and effective i..., J. Control. Release (2016), http://dx.doi.org/10.1016/j.jconrel.2016.12.011

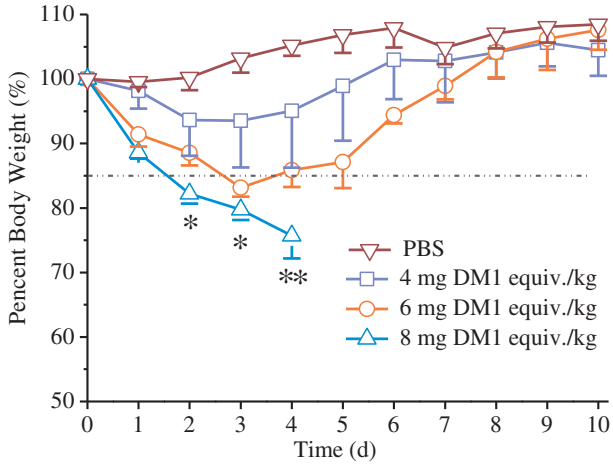

Fig. 6. MTD studies of cRGD-MMP in C57BL/6 mice (n = 5). Mice treated with PBS were used as control. * Indicates one mouse died.

3. Results and discussion

3.1. Synthesis of PEG-P(TMC-g-SSDM1) and cRGD-PEG- P(TMC-g-SSDM1) copolymers

PEG-P(TMC-*g*-SSDM1) copolymer was obtained by ring-opening copolymerization of trimethylene carbonate (TMC) and pyridyl disulfide carbonate (PDSC) using PEG-OH (M_n = 5.0 kg/mol) as an initiator followed by thiol-disulfide exchange with DM1 (Scheme 2). The polymerization was conducted in DCM at 40 °C for 24 h using zinc bis[bis(trimethylsilyl) amide] as a catalyst. ^{1}H NMR of PEG-P(TMC-*co*-PDSC) detected signals assignable to PEG at δ 3.65 and 3.38, TMC moieties at δ 4.24 and 2.05, as well as PDSC moieties at δ 8.46, 7.65, 7.09, 4.11, 3.01, 1.12 (Fig. 1A). The degree of polymerizations (DP) of TMC and PDSC was calculated to be 39 and 10.5 by comparing signals at δ 2.05 and 8.46 with that at δ 3.65, respectively, corresponding to an M_n of 11.8 kg/mol (Table S1). UV–vis measurement of pyridine-2-thione released from PEG-P(TMC-*co*-PDSC) after excess DTT treatment confirmed ca. 10.8 units of PDSC per polymer chain (Table S1). The conversion of TMC monomer was nearly quantitative while PDSC monomer had a conversion of ca. 65% (Table S1), indicating that TMC has a higher reactivity than PDSC. The relatively lower reactivity of PDSC likely arises from its steric hindrance. GPC showed that PEG-P(TMC-*co*-PDSC) had an M_n of 23.3 kg/mol and a moderate M_w/M_n of 1.53 (Table S1).

The thiol-disulfide exchange reaction was carried out at a DM1/PDSC molar ratio of 3/2 in DMF at 35 °C for 48 h in the presence of glacial acetic acid (Scheme 2). ^{1}H NMR of PEG-P(TMC-*g*-SSDM1) revealed that signals at δ 8.46 and 7.65 attributable to the aromatic protons of PDSC moieties completely disappeared and new peaks due to DM1 were discerned at δ 7.16, 6.89, 6.54, 5.92, 5.56, 5.30, 4.53, indicating successful conjugation of DM1 (Fig. 1B). Taking advantage of the quantitative thiol-disulfide exchange with PDSC moieties, we have prepared poly(ε-caprolactone)-*g*-SS-PEG and poly(ε-caprolactone)-*g*-SS-lactobionic acid copolymers [48,51]. The comparison of signal at δ 7.16 (aromatic protons of DM1) with signal at δ 1.94 (methylene protons of TMC and methyl protons of DM1) and δ 3.50 (methylene protons of

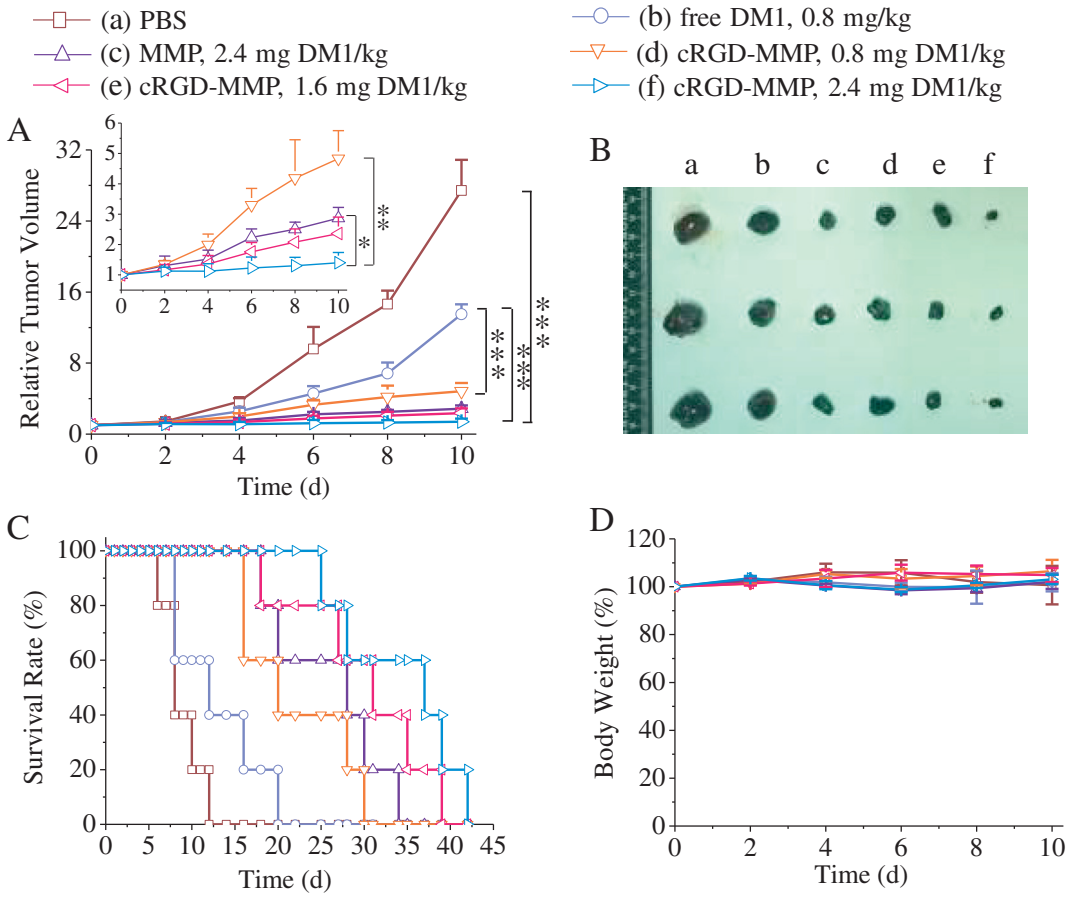

Fig. 7. (A) Tumor volume changes of B16F10 tumor bearing C57BL/6 mice treated with free DM1, MMP and cRGD-MMP, respectively. DM1 drugs were given on day 0, 2 and 4 for a total of three injections. The results were presented as mean ± standard deviation (n = 8). *p < 0.05, **p < 0.01, ***p < 0.001 (student's *t*-test). (B) Photographs of typical tumor blocks collected from different treatment groups on day 10. (C) Survival rates of mice in different treatment groups within 45 d. (D) Change of mice body weights in 10 d following different treatments.

Please cite this article as: P. Zhong, et al., αvβ3 Integrin-targeted reduction-sensitive micellar mertansine prodrug: Superb drug loading, enhanced stability, and effective i..., J. Control. Release (2016), http://dx.doi.org/10.1016/j.jconrel.2016.12.011

PEG and methylene and methyl protons of DM1) showed a remarkably high DM1 content of about 40.2 *wt.%*. HPLC results showed that DM1 content in the prodrug was about 40.0 *wt.%*, close to that determined by ^{1}H NMR analysis (Fig. S1). HPLC curves showed absence of free DM1 in PEG-P(TMC-*g*-SSDM1) prodrug, supporting complete removal of free drug. In contrast, antibody-maytansinoid conjugates (AMCs) have a typically low drug loading of <2.5 *wt.%* [10,52]. The clinically used ado-trastuzumab emtansine (T-DM1) was reported to contain ca. 1.8 *wt.%* DM1 [53]. The superior drug content of PEG-P(TMC-*g*-SSDM1) prodrug would greatly reduce the amount of carriers and injection volume.

cRGD-PEG-P(TMC-*g*-SSDM1) copolymer was prepared by copolymerization of TMC and PDSC using Mal-PEG-OH (M_n = 5.0 kg/mol) as a macro-initiator followed by Michael-type addition reaction with Cyclo(RGD*f*C) peptide and thiol-disulfide exchange with DM1 (Scheme S1). ^{1}H NMR revealed that TMC and PDSC in Mal-PEG-P(TMC-*co*-PDSC) copolymer had DP of 39 and 11, respectively, corresponding to an M_n of 12.0 kg/mol, close to that of PEG-P(TMC-*co*-PDSC) (Fig. S2A, Table S1). GPC showed that Mal-PEG-P(TMC-*co*-PDSC) had an M_n of 26.1 kg/mol and a PDI of 1.42 (Table S1). In order to prevent the thiol-disulfide exchange reaction between cRGD-SH and PDSC, cRGD-SH was conjugated to Mal-PEG-P(TMC-*co*-PDSC) micelles in water at room temperature for 24 h. ^{1}H NMR displayed complete disappearance of signals at δ 6.70 assignable to Mal groups (Fig. S2B). Micro BCA protein assay kit (Thermo Scientific) confirmed quantitative conjugation of cRGD. It should be noted that no alternation of signals at δ 8.46 and 7.65 assignable to the pyridyl protons of PDSC was observed (Fig. S2B), demonstrating that pyridyldisulfide functional groups are intact. The thiol-disulfide exchange between cRGD-PEG-P(TMC-*co*-PDSC) and DM1 yielded cRGD-PEG-P(TMC-*g*-SSDM1) with a DM1 content of 40.6 *wt.%* as determined by ^{1}H NMR (Fig. S4) and 40.3 *wt.%* by HPLC measurements (Fig. S1).

3.2. Preparation and reduction-triggered drug release of cRGD-MMP

The co-self-assembly of cRGD-PEG-P(TMC-*g*-SSDM1) and PEG-P(TMC-*g*-SSDM1) copolymers (w/w 20/80) in water furnished cRGD-MMP with a small size of 45 nm and a low polydispersity index (PDI) of 0.11 (Fig. 2A). TEM confirmed that cRGD-MMP had a small size and spherical morphology (Fig. 2B). cRGD-MMP exhibited a low critical micelle concentration (CMC) of 4.76 mg/L, as determined by fluorescence measurements using pyrene as a probe (Fig. S4A). Notably, no change of size was observed for cRGD-MMP in 10% FBS and DMEM cell culture medium in 24 h (Fig. 2C), indicating that cRGD-MMP has excellent colloidal stability. However, under a reductive environment containing

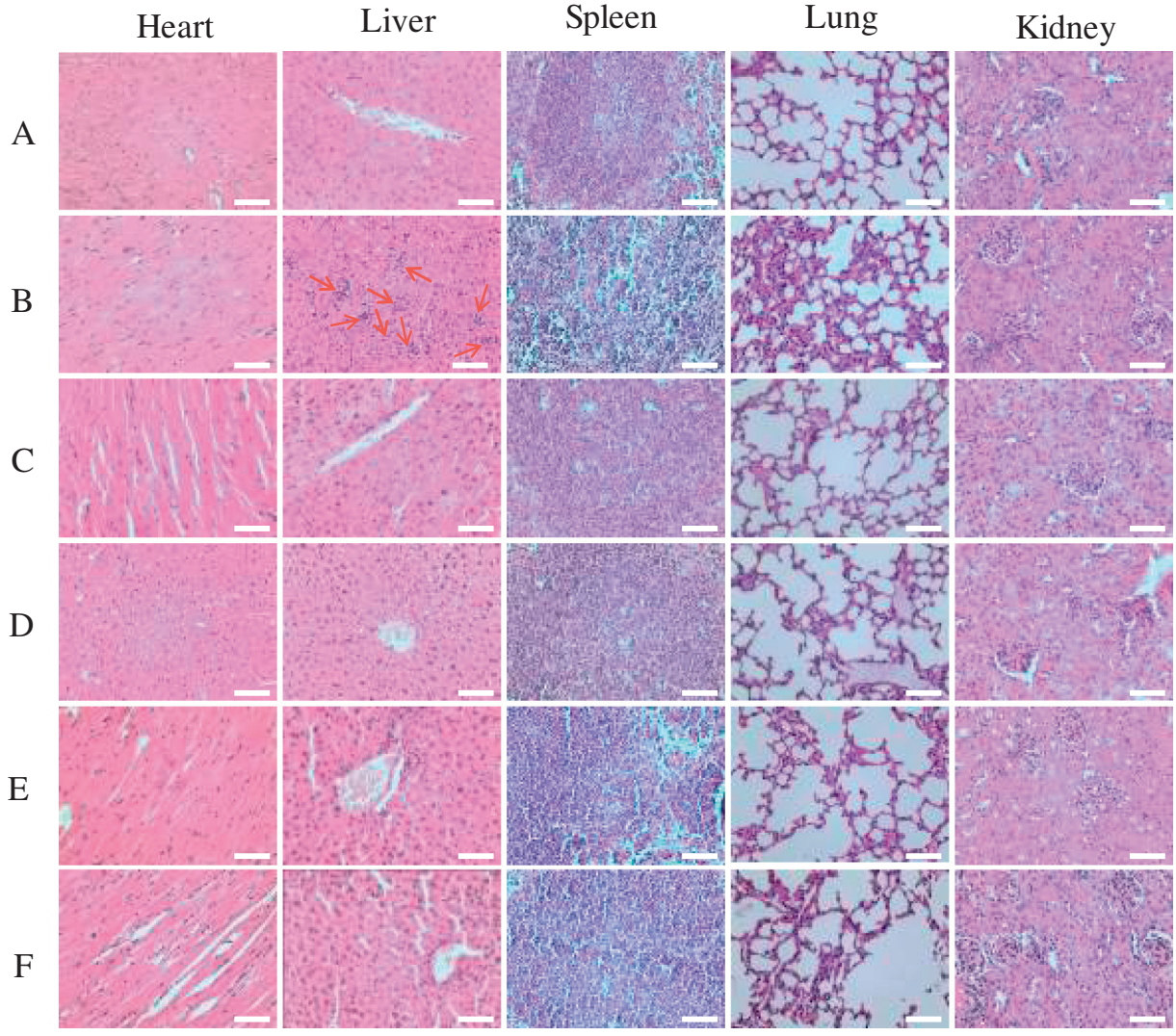

Fig. 8. H&E staining of mice major organs from different groups. (A) PBS; (B) free DM1, 0.8 mg/kg; (C) MMP, 2.4 mg DM1/kg; (D) cRGD-MMP, 0.8 mg DM1/kg; (E) cRGD-MMP, 1.6 mg DM1/kg; and (F) cRGD-MMP, 2.4 mg DM1/kg. The red arrows in the liver tissue of group B indicate the obvious increased Kupffer cells, leading to liver damage. The images were acquired using Olympus BX41 microscope at 40× objective (scale bar: 50 μm). (For interpretation of the references to color in this figure legend, the reader is referred to the web version of this article.)

Please cite this article as: P. Zhong, et al., αvβ3 Integrin-targeted reduction-sensitive micellar mertansine prodrug: Superb drug loading, enhanced stability, and effective i..., J. Control. Release (2016), http://dx.doi.org/10.1016/j.jconrel.2016.12.011

10 mM GSH, cRGD-MMP swelled from 40 nm to over 600 nm in 24 h with PDI increased from 0.1 to over 0.5 (Fig. 2D). In a similar way, we have also obtained non-targeting MMP by self-assembly of PEG-P(TMC-*g*-SSDM1) alone. MMP exhibited similar size distribution (39 nm, PDI = 0.09, Fig. S5) and CMC (4.16 mg/L, Fig. S4B) to cRGD-MMP.

The in vitro release studies showed fast release of DM1 from cRGD-MMP in the presence of 10 mM GSH, in which over 55% and 80% DM1 was released in 6 and 24 h, respectively (Fig. 3). In contrast, little DM1 (<10%) was released in 24 h under a non-reductive condition. These results support that cRGD-MMP has excellent stability with inhibited premature drug release under physiological environment while is capable of releasing DM1 under cytoplasmic reducing condition. It should be noted that released DM1 is in its pristine form, which guarantees fully preserving its antitumor activity. MMP displayed a similar release profile to cRGD-MMP (Fig. 3), indicating that conjugation of cRGD peptide does not affect its drug release behavior.

3.3. Anticancer effect of cRGD-MMP to B16F10 cells in vitro

The in vitro anticancer activity of cRGD-MMP and MMP was assessed using MTT assays in $\alpha_v\beta_3$ integrin overexpressing B16F10 cancer cells. Notably, cRGD-MMP displayed a remarkably low IC_{50} of 0.16 μg DM1 equiv./mL, which was close to that of DM1 and 2.7-fold lower than that of MMP (Fig. 4A), supporting that cRGD-MMP has obvious targetability to B16F10 cells.

To investigate their cellular uptake behaviors in B16F10 cells, cRGD-MMP was loaded with doxorubicin (fluorescent anticancer drug) and studied using flow cytometry and confocal laser scanning microscopy (CLSM). Flow cytometry showed that B16F10 cells following 4 h incubation with DOX-loaded cRGD-MMP exhibited a nearly 3-fold higher cellular DOX level than those with MMP under otherwise the same conditions (Fig. 4B), confirming the active role of cRGD in mediating cellular uptake. CLSM images revealed that cells treated with DOX-loaded cRGD-MMP showed much stronger intracellular DOX fluorescence than those treated with MMP (Fig. 4C). The fluorescence of DOX would be self-quenched when encapsulated inside the micelles [54,55]. The observed strong DOX fluorescence in B16F10 cells indicates not only efficient internalization of cRGD-MMP by B16F10 cells but also fast intracellular drug release. This study further demonstrates that cRGD-MMP can be applied as a nanovehicle for co-delivery of other lipophilic drugs, which might achieve synergistic treatment effects [56,57].

3.4. Blood circulation, toleration and antitumor efficacy of cRGD-MMP in vivo

To study their in vivo pharmacokinetics, cRGD-MMP and MMP were *i.v.* injected into healthy C57BL/6 mice at 5 mg DM1 equiv./kg and plasma DM1 levels at different time intervals were determined by HPLC. Interestingly, both cRGD-MMP and MMP had a long circulation time with an elimination half-life of 5.69 h and 5.25 h, respectively (Fig. 5). It should be noted that there was no difference in blood clearance profiles for cRGD-MMP and MMP, indicating that cRGD decoration does not alter their pharmacokinetics.

The clinical use of DM1 is limited by its low therapeutic window [52]. To assess its therapeutic index, the maximum-tolerated dose (MTD) of cRGD-MMP and MMP was determined in C57BL/6 mice. The results showed that both cRGD-MMP and MMP exhibited an MTD of over 4 mg DM1 equiv./kg (Fig. 6, Fig. S6A), which is at least 4-fold higher than free DM1 (Fig. S6B). It should be noted that disulfide-linked antibody-maytansinoid conjugates (AMCs) have an MTD of about 0.9 mg DM1 equiv./kg while AMCs with non-cleavable linkers exhibit an MTD of about 2.7 mg DM1 equiv./kg [10]. The better toleration of cRGD-MMP is most likely due to its enhanced colloidal stability, inhibited DM1 leakage, and reduced off-target accumulation.

To evaluate its in vivo anticancer effects, cRGD-MMP was administrated into B16F10 tumor-bearing C57BL/6 mice every two days for a total of three injections at 0.8, 1.6 or 2.4 mg DM1 equiv./kg. As expected, PBS treated mice showed aggressive tumor growth (Fig. 7A). Free DM1 displayed modest tumor growth inhibition at a dose of 0.8 mg/kg. Considering that free DM1 has an MTD of 1 mg/kg, no higher dosage was attempted. cRGD-MMP displayed significantly better tumor suppression at 0.8 mg/kg than free DM1 under otherwise the same conditions. Moreover, cRGD-MMP exhibited a dose-dependent tumor growth inhibition, in which tumor progression was completely suppressed at 2.4 mg DM1 equiv./kg. It should further be noted that the non-targeted MMP showed also effective inhibition of tumor growth at 2.4 mg DM1 equiv./kg, though to a less extent than cRGD-MMP. On day 10, three mice of each group were sacrificed and tumors were collected, weighed and photographed. The remaining five mice of each group were used to monitor survival rate. The images of tumors showed clearly that mice treated with 2.4 mg DM1 equiv./kg cRGD-MMP had the smallest tumor size (Fig. 7B), supporting that cRGD-MMP leads to the most efficient tumor growth inhibition. The weights of tumor blocks indicate that cRGD-MMP yielded tumor inhibition rate (TIR) of 82.2%, 89.6% and 97.5% at 0.8, 1.6 or 2.4 mg DM1 equiv./kg, respectively (Fig. S7). MMP at 2.4 mg DM1 equiv./kg also exhibited a considerable TIR of 87.5%. In line with tumor inhibition results, mice treated with cRGD-MMP and MMP exhibited much better survival rates as compared to those with free DM1 (Fig. 7C). The median survival times were 20, 31 and 37 days for mice treated with 0.8, 1.6 and 2.4 mg DM1 equiv./kg cRGD-MMP, respectively. Mice treated with 2.4 mg DM1 equiv./kg MMP had a prolonged median survival time of 28 days. In contrast, free DM1 exhibited a much shorter median survival time of 12 days. Notably, all of the treatments were well tolerated by mice as evidenced by little body weight change over the entire experimental period (Fig. 7D). H&E staining (Fig. 8) displayed that cRGD-MMP at 0.8–2.4 mg DM1 equiv./kg did not cause significant damage to the main organs while free DM1 induced obvious liver damage, in line with the report that DM1 had a high cytotoxic potency in liver [10]. All the above results demonstrate that cRGD-MMP has improved toleration, better selectivity and enhanced treatment of B16F10 melanoma. The superb drug loading, high stability, easy fabrication and quick intracellular drug release renders cRGD-MMP a potentially superior substitute to antibody-drug conjugates.

4. Conclusions

cRGD-functionalized and reduction-sensitive polymeric micellar mertansine prodrug (cRGD-MMP) mediates targeted treatment of malignant B16F10 melanoma-bearing C57BL/6 mice, resulting in effective suppression of tumor growth and significantly improved survival rate. cRGD-MMP has uniquely combined both features of polymeric prodrugs and micellar drugs, presenting the following multi-functions: superb drug loading content (about 40 *wt*.%), high stability, decreased systemic toxicity, fast intracellular activation, long circulation time, and active targeting effect to $\alpha_v\beta_3$ integrin over-expressing B16F10 melanoma cancer cells. Notably, unlike antibody-drug conjugates, cRGD-MMP can be easily manufactured in a large scale and at a low cost. This smart micellar mertansine prodrug appears as a potentially better and safer substitute to antibody-maytansinoid conjugates for targeted chemotherapy of $\alpha_v\beta_3$ integrin-overexpressing malignancies.

Acknowledgments

This work was supported by the National Natural Science Foundation of China (NSFC 51373113, 51225302, 51633005), the Natural Science Foundation of Jiangsu Province (BK20131166), a Project Funded by the Priority Academic Program Development of Jiangsu Higher Education Institutions.

Please cite this article as: P. Zhong, et al., αvβ3 Integrin-targeted reduction-sensitive micellar mertansine prodrug: Superb drug loading, enhanced stability, and effective i..., J. Control. Release (2016), http://dx.doi.org/10.1016/j.jconrel.2016.12.011

Appendix A. Supplementary data

Supplementary data to this article can be found online at http://dx.doi.org/10.1016/j.jconrel.2016.12.011.

References

[1] A. Thomas, B.A. Teicher, R. Hassan, Antibody–drug conjugates for cancer therapy, Lancet Oncol. 17 (2016) e254–e262.
[2] E.L. Sievers, P.D. Senter, Antibody-drug conjugates in cancer therapy, Annu. Rev. Med. 64 (2013) 15–29.
[3] S. Verma, D. Miles, L. Gianni, I.E. Krop, M. Welslau, J. Baselga, M. Pegram, D.-Y. Oh, V. Diéras, E. Guardino, Trastuzumab emtansine for HER2-positive advanced breast cancer, N. Engl. J. Med. 367 (2012) 1783–1791.
[4] L. Amiri-Kordestani, G.M. Blumenthal, Q.C. Xu, L. Zhang, S.W. Tang, L. Ha, W.C. Weinberg, B. Chi, R. Candau-Chacon, P. Hughes, FDA approval: ado-trastuzumab emtansine for the treatment of patients with HER2-positive metastatic breast cancer, Clin. Cancer Res. 20 (2014) 4436–4441.
[5] K. Traynor, Ado-trastuzumab emtansine approved for advanced breast cancer, Am. J. Health Syst. Pharm. 70 (2013) 562.
[6] V. Chudasama, A. Maruani, S. Caddick, Recent advances in the construction of antibody-drug conjugates, Nat. Chem. 8 (2016) 114–119.
[7] M.H. Shah, P. Lorigan, M.E. O'Brien, F.V. Fossella, K.N. Moore, S. Bhatia, M. Kirby, P.J. Woll, Phase I study of IMGN901, a CD56-targeting antibody-drug conjugate, in patients with CD56-positive solid tumors, Investig. New Drugs 34 (2016) 290–299.
[8] B.E.D. Goeij, J.M. Lambert, New developments for antibody-drug conjugate-based therapeutic approaches, Curr. Opin. Immunol. 40 (2016) 14–23.
[9] H.L. Perez, P.M. Cardarelli, S. Deshpande, S. Gangwar, G.M. Schroeder, G.D. Vite, R.M. Borzilleri, Antibody–drug conjugates: current status and future directions, Drug Discov. Today 19 (2014) 869–881.
[10] R.V. Chari, M.L. Miller, W.C. Widdison, Antibody–drug conjugates: an emerging concept in cancer therapy, Angew. Chem. Int. Ed. 53 (2014) 3796–3827.
[11] M.J. Hinrichs, R. Dixit, Antibody drug conjugates: nonclinical safety considerations, AAPS J. 17 (2015) 1055–1064.
[12] R. Duncan, M.J. Vicent, Polymer therapeutics-prospects for 21st century: the end of the beginning, Adv. Drug Deliv. Rev. 65 (2013) 60–70.
[13] K. Ulbrich, K.i. Holá, V. Šubr, A. Bakandritsos, J.i. Tuček, R. Zbořil, Targeted drug delivery with polymers and magnetic nanoparticles: covalent and noncovalent approaches, release control, and clinical studies, Chem. Rev. 116 (2016) 5338–5431.
[14] C. Li, S. Wallace, Polymer-drug conjugates: recent development in clinical oncology, Adv. Drug Deliv. Rev. 60 (2008) 886–898.
[15] J. Sanchis, F. Canal, R. Lucas, M.J. Vicent, Polymer-drug conjugates for novel molecular targets, Nanomedicine 5 (2010) 915–935.
[16] Y. Yuan, L. Jie, B. Liu, Conjugated-polyelectrolyte-based polyprodrug: targeted and image-guided photodynamic and chemotherapy with on-demand drug release upon irradiation with a single light source, Angew. Chem. Int. Ed. 53 (2014) 7163–7168.
[17] S. Dragojevic, J.S. Ryu, D. Raucher, Polymer-based prodrugs: improving tumor targeting and the solubility of small molecule drugs in cancer therapy, Molecules 20 (2015) 21750–21769.
[18] L.W. Seymour, D.R. Ferry, D.J. Kerr, D. Rea, M. Whitlock, R. Poyner, C. Boivin, S. Hesslewood, C. Twelves, R. Blackie, Phase II studies of polymer-doxorubicin (PK1, FCE28068) in the treatment of breast, lung and colorectal cancer, Int. J. Oncol. 34 (2009) 1629–1636.
[19] O. Soepenberg, M.J. de Jonge, A. Sparreboom, P. de Bruin, F.A. Eskens, G. de Heus, J. Wanders, P. Cheverton, M.P. Ducharme, J. Verweij, Phase I and pharmacokinetic study of DE-310 in patients with advanced solid tumors, Clin. Cancer Res. 11 (2005) 703–711.
[20] G.J. Weiss, J. Chao, J.D. Neidhart, R.K. Ramanathan, D. Bassett, J.A. Neidhart, C.H.J. Choi, W. Chow, V. Chung, S.J. Forman, First-in-human phase 1/2a trial of CRLX101, a cyclodextrin-containing polymer-camptothecin nanopharmaceutical in patients with advanced solid tumor malignancies, Investig. New Drugs 31 (2013) 986–1000.
[21] M. Mita, A. Mita, J. Sarantopoulos, C.H. Takimoto, E.K. Rowinsky, O. Romero, P. Angiuli, C. Allievi, A. Eisenfeld, C.F. Verschraegen, Phase I study of paclitaxel poliglumex administered weekly for patients with advanced solid malignancies, Cancer Chemother. Pharmacol. 64 (2009) 287–295.
[22] R. Mahato, W. Tai, K. Cheng, Prodrugs for improving tumor targetability and efficiency, Adv. Drug Deliv. Rev. 63 (2011) 659–670.
[23] C.M. Dawidczyk, C. Kim, J.H. Park, L.M. Russell, K.H. Lee, M.G. Pomper, P.C. Searson, State-of-the-art in design rules for drug delivery platforms: lessons learned from FDA-approved nanomedicines, J. Control. Release 187 (2014) 133–144.
[24] X. Zhang, K. Achazi, D. Steinhilber, F. Kratz, J. Dernedde, R. Haag, A facile approach for dual-responsive prodrug nanogels based on dendritic polyglycerols with minimal leaching, J. Control. Release 174 (2014) 209–216.
[25] H. Han, H. Wang, Y. Chen, Z. Li, Y. Wang, Q. Jin, J. Ji, Theranostic reduction-sensitive gemcitabine prodrug micelles for near-infrared imaging and pancreatic cancer therapy, Nanoscale 8 (2016) 283–291.
[26] Y. Bao, M. Yin, X. Hu, X. Zhuang, Y. Sun, Y. Guo, S. Tan, Z. Zhang, A safe, simple and efficient doxorubicin prodrug hybrid micelle for overcoming tumor multidrug resistance and targeting delivery, J. Control. Release 235 (2016) 182–194.
[27] P. Huang, D. Wang, Y. Su, W. Huang, Y. Zhou, D. Cui, X. Zhu, D. Yan, Combination of small molecule prodrug and Nanodrug delivery: amphiphilic drug–drug conjugate for cancer therapy, J. Am. Chem. Soc. 136 (2014) 11748–11756.
[28] J. Mao, Y. Li, T. Wu, C. Yuan, B. Zeng, Y. Xu, L. Dai, A simple dual-pH responsive prodrug-based polymeric micelles for drug delivery, ACS Appl. Mater. Interfaces 8 (2016) 17109–17117.
[29] L. Zhu, T. Wang, F. Perche, A. Taigind, V.P. Torchilin, Enhanced anticancer activity of nanopreparation containing an MMP2-sensitive PEG-drug conjugate and cell-penetrating moiety, Proc. Natl. Acad. Sci. U. S. A. 110 (2013) 17047–17052.
[30] Y. Zhong, K. Goltsche, L. Cheng, F. Xie, F. Meng, C. Deng, Z. Zhong, R. Haag, Hyaluronic acid-shelled acid-activatable paclitaxel prodrug micelles effectively target and treat CD44-overexpressing human breast tumor xenografts in vivo, Biomaterials 84 (2016) 250–261.
[31] W.C. Widdison, S.D. Wilhelm, E.E. Cavanagh, K.R. Whiteman, B.A. Leece, Y. Kovtun, V.S. Goldmacher, H. Xie, R.M. Steeves, R.J. Lutz, Semisynthetic maytansine analogues for the targeted treatment of cancer, J. Med. Chem. 49 (2006) 4392–4408.
[32] R. Cheng, F. Meng, C. Deng, Z. Zhong, Bioresponsive polymeric nanotherapeutics for targeted cancer chemotherapy, Nano Today 10 (2015) 656–670.
[33] M. Huo, J. Yuan, L. Tao, Y. Wei, Redox-responsive polymers for drug delivery: from molecular design to applications, Polym. Chem. 5 (2014) 1519–1528.
[34] R. Mo, Z. Gu, Tumor microenvironment and intracellular signal-activated nanomaterials for anticancer drug delivery, Mater. Today 19 (2016) 274–283.
[35] W. Yang, Y. Zou, F. Meng, J. Zhang, R. Cheng, C. Deng, Z. Zhong, Efficient and targeted suppression of human lung tumor xenografts in mice with methotrexate sodium encapsulated in all-function-in-one chimeric polymersomes, Adv. Mater. (2016)http://dx.doi.org/10.1002/adma.201600065.
[36] X.-D. Xu, Y.-J. Cheng, J. Wu, H. Cheng, S.-X. Cheng, R.-X. Zhuo, X.-Z. Zhang, Smart and hyper-fast responsive polyprodrug nanoplatform for targeted cancer therapy, Biomaterials 76 (2016) 238–249.
[37] H.-C. Yen, H. Cabral, P. Mi, K. Toh, Y. Matsumoto, X. Liu, H. Koori, A. Kim, K. Miyazaki, Y. Miura, Light-induced cytosolic activation of reduction-sensitive camptothecin-loaded polymeric micelles for spatiotemporally controlled in vivo chemotherapy, ACS Nano 8 (2014) 11591–11602.
[38] D. Li, Y. Bu, L. Zhang, X. Wang, Y. Yang, Y. Zhuang, F. Yang, H. Shen, D.C. Wu, Facile construction of pH- and redox-responsive micelles from a biodegradable poly(β-hydroxyl amine) for drug delivery, Biomacromolecules 17 (2015) 291–300.
[39] W. Chen, F. Meng, R. Cheng, C. Deng, J. Feijen, Z. Zhong, Advanced drug and gene delivery systems based on functional biodegradable polycarbonates and copolymers, J. Control. Release 190 (2014) 398–414.
[40] K. Fukushima, Poly (trimethylene carbonate)-based polymers engineered for biodegradable functional biomaterials, Biomater. Sci. 4 (2016) 9–24.
[41] Y. Zhong, F. Meng, C. Deng, Z. Zhong, Ligand-directed active tumor-targeting polymeric nanoparticles for cancer chemotherapy, Biomacromolecules 15 (2014) 1955–1969.
[42] Y. Miura, T. Takenaka, K. Toh, S. Wu, H. Nishihara, M.R. Kano, Y. Ino, T. Nomoto, Y. Matsumoto, H. Koyama, Cyclic RGD-linked polymeric micelles for targeted delivery of platinum anticancer drugs to glioblastoma through the blood–brain tumor barrier, ACS Nano 7 (2013) 8583–8592.
[43] N. Graf, D.R. Bielenberg, N. Kolishetti, C. Muus, J. Banyard, O.C. Farokhzad, S.J. Lippard, αVβ3 Integrin-targeted PLGA-PEG nanoparticles for enhanced anti-tumor efficacy of a Pt (IV) prodrug, ACS Nano 6 (2012) 4530–4539.
[44] K. Shi, J. Li, Z. Cao, P. Yang, Y. Qiu, B. Yang, Y. Wang, Y. Long, Y. Liu, Q. Zhang, A pH-responsive cell-penetrating peptide-modified liposomes with active recognizing of integrin α v β 3 for the treatment of melanoma, J. Control. Release 217 (2015) 138–150.
[45] Y. Guo, B. Niu, Q. Song, Y. Zhao, Y. Bao, S. Tan, L. Si, Z. Zhang, RGD-decorated redox-responsive d-α-tocopherol polyethylene glycol succinate–poly (lactide) nanoparticles for targeted drug delivery, J. Mater. Chem. B 4 (2016) 2338–2350.
[46] G. Chen, L. Wang, T. Cordie, C. Vokoun, K.W. Eliceiri, S. Gong, Multi-functional self-fluorescent unimolecular micelles for tumor-targeted drug delivery and bioimaging, Biomaterials 47 (2015) 41–50.
[47] K.J. Hamblett, C.J. Kozlosky, S. Siu, W.S. Chang, H. Liu, I.N. Foltz, E.S. Trueblood, D. Meininger, T. Arora, B. Twomey, AMG 595, an anti-EGFRvIII antibody-drug conjugate, induces potent antitumor activity against EGFRvIII-expressing glioblastoma, Mol. Cancer Ther. 14 (2015) 1614–1624.
[48] W. Chen, Y. Zou, J. Jia, F. Meng, R. Cheng, C. Deng, J. Feijen, Z. Zhong, Functional poly (ε-caprolactone) s via copolymerization of ε-caprolactone and pyridyl disulfide-containing cyclic carbonate: controlled synthesis and facile access to reduction-sensitive biodegradable graft copolymer micelles, Macromolecules 46 (2013) 699–707.
[49] A. Banzato, S. Bobisse, M. Rondina, D. Renier, F. Bettella, G. Esposito, L. Quintieri, L. Meléndez-Alafort, U. Mazzi, P. Zanovello, A paclitaxel-hyaluronan bioconjugate targeting ovarian cancer affords a potent in vivo therapeutic activity, Clin. Cancer Res. 14 (2008) 3598–3606.
[50] S. Liu, J. Liu, Q. Ma, L. Cao, R.J. Fattah, Z. Yu, T.H. Bugge, T. Finkel, S.H. Leppla, Solid tumor therapy by selectively targeting stromal endothelial cells, Proc. Natl. Acad. Sci. U. S. A. 113 (2016) E4079–E4087.
[51] W. Chen, Y. Zou, F. Meng, R. Cheng, C. Deng, J. Feijen, Z. Zhong, Glyco-nanoparticles with sheddable saccharide shells: a unique and potent platform for hepatoma-targeting delivery of anticancer drugs, Biomacromolecules 15 (2014) 900–907.
[52] R.V. Chari, Targeted cancer therapy: conferring specificity to cytotoxic drugs, Acc. Chem. Res. 41 (2007) 98–107.
[53] G.D.L. Phillips, G. Li, D.L. Dugger, L.M. Crocker, K.L. Parsons, E. Mai, W.A. Blättler, J.M. Lambert, R.V. Chari, R.J. Lutz, Targeting HER2-positive breast cancer with trastuzumab-DM1, an antibody–cytotoxic drug conjugate, Cancer Res. 68 (2008) 9280–9290.

Please cite this article as: P. Zhong, et al., αvβ3 Integrin-targeted reduction-sensitive micellar mertansine prodrug: Superb drug loading, enhanced stability, and effective i..., J. Control. Release (2016), http://dx.doi.org/10.1016/j.jconrel.2016.12.011

[54] J. Xiong, F. Meng, C. Wang, R. Cheng, Z. Liu, Z. Zhong, Folate-conjugated crosslinked biodegradable micelles for receptor-mediated delivery of paclitaxel, J. Mater. Chem. 21 (2011) 5786–5794.
[55] Y. Zhu, Z. Jian, F. Meng, D. Chao, C. Ru, J. Feijen, Z. Zhong, cRGD-functionalized reduction-sensitive shell-sheddable biodegradable micelles mediate enhanced doxorubicin delivery to human glioma xenografts in vivo, J. Control. Release 233 (2016) 29–38.
[56] Y. Zhang, C. Yang, W. Wang, J. Liu, Q. Liu, F. Huang, L. Chu, H. Gao, C. Li, D. Kong, Co-delivery of doxorubicin and curcumin by pH-sensitive prodrug nanoparticle for combination therapy of cancer, Sci. Rep. 6 (2016)http://dx.doi.org/10.1038/srep21225.
[57] W. Tai, R. Mo, Y. Lu, T. Jiang, Z. Gu, Folding graft copolymer with pendant drug segments for co-delivery of anticancer drugs, Biomaterials 35 (2014) 7194–7203.

Please cite this article as: P. Zhong, et al., αvβ3 Integrin-targeted reduction-sensitive micellar mertansine prodrug: Superb drug loading, enhanced stability, and effective i..., J. Control. Release (2016), http://dx.doi.org/10.1016/j.jconrel.2016.12.011